On the Effects of Bremsstrahlung Radiation during Energetic Electron Precipitation

Wei Xu,[1] Robert A. Marshall,[1] Xiaohua Fang,[2] Esa Turunen,[3] and Antti Kero[3,4]

[1]Department of Aerospace Engineering Sciences, University of Colorado Boulder, Boulder, Colorado, USA.
[2]Laboratory for Atmospheric and Space Physics, University of Colorado Boulder, Boulder, Colorado, USA.
[3]Sodankylä Geophysical Observatory, University of Oulu, Oulu, Finland.
[4]Institute of Space-Earth Environmental Research, Nagoya University, Nagoya, Japan.

Key Points:

- The energy and altitude distributions of bremsstrahlung photons produced during electron precipitation have been quantified.
- The ionization rate due to both precipitating electrons and associated bremsstrahlung photons has been calculated.
- Bremsstrahlung-induced chemical impacts on the atmosphere during realistic electron precipitation are likely insignificant.

Corresponding author: Wei Xu, Wei-Xu@colorado.edu

Abstract

Precipitation of energetic particles into the Earth's atmosphere can significantly change the properties, dynamics, as well as the chemical composition of the upper and middle atmosphere. In this paper, using Monte Carlo models, we simulate, from first principles, the interaction of monoenergetic beams of precipitating electrons with the atmosphere, with particular emphasis on the process of bremsstrahlung radiation and its resultant ionization production and atmospheric effects. The pitch angle dependence of the ionization rate profile has been quantified: the altitude of peak ionization rate depends on the pitch angle by a few kilometers. We also demonstrate that the transport of precipitating electron energy in the form of bremsstrahlung photons leads to ionization at altitudes significantly lower than the direct impact ionization, as low as ~20 km for 1 MeV precipitating electrons. Moreover, chemical modeling results suggest that the chemical effects in the atmosphere due to bremsstrahlung-induced ionization production during energetic electron precipitation are likely insignificant.

1 Introduction

Precipitation of energetic particles into the Earth's atmosphere can significantly change the properties, dynamics, as well as the chemical composition of the upper and middle atmosphere. The energy deposited by energetic particle precipitation (EPP) is responsible for sustaining the D-region ionospheric properties on the night side, which is integrally important in a number of areas in heliophysics, aeronomy, and long-range communications [e.g., *Barr et al.*, 2000]. Moreover, through various dynamical and chemical processes, EPP results in efficient production of reactive odd nitrogen [e.g., *Rusch et al.*, 1981] and odd hydrogen [e.g., *Solomon et al.*, 1981], both of which are capable of depleting ozone in the stratosphere and mesosphere [e.g., *Thorne*, 1980; *Randall et al.*, 2007; *Sinnhuber et al.*, 2012; *Rozanov et al.*, 2012; *Andersson et al.*, 2013; *Seppälä et al.*, 2015]. For a single pulsating aurora event, chemical modeling studies have revealed that the high-energy component of electron precipitation can deplete the mesospheric odd oxygen by up to several tens of percent [*Turunen et al.*, 2016].

Given the above-mentioned importance, various numerical techniques have been developed in order to study the interaction of energetic electron precipitation (EEP) with the upper atmosphere, including parameterization methods [e.g., *Roble and Ridley*, 1987; *Lummerzheim*, 1992; *Fang et al.*, 2008, 2010] and physics-based Monte Carlo simulations [e.g., *Solomon*, 2001; *Cotts et al.*, 2011]. Using empirical auroral ionization profiles [*Lazarev*, 1967], *Roble and Ridley* [1987] developed a parameterization method for the National Center for Atmospheric Research (NCAR) thermospheric general circulation model. This method was further improved by *Lummerzheim* [1992] and a new set of parameterization coefficients was reported, and later adopted in the Whole Atmosphere Community Climate Model (WACCM) [*Garcia et al.*, 2007]. Furthermore, based on first-principle models, *Fang et al.* [2008, 2010] have proposed new parameterization schemes and greatly extended the energy range of precipitating electrons. On the other hand, *Solomon* [2001] has developed a Monte Carlo model and investigated the collisional processes during auroral particle transport.

Accurate modeling of electron precipitation is of crucial importance, especially for the estimation of its influence on the electrical and chemical properties of the Earth's atmosphere using space-borne and ground-based observations. However, previous modeling studies were mainly dedicated to the direct impact ionization by precipitating electrons. The secondary ionization effects induced by bremsstrahlung photons, which are significant for relativistic precipitating electrons and particularly at low altitudes (<50 km) [*Frahm et al.*, 1997], have not been sufficiently studied. These effects have been long suggested to have implications for the increase of stratospheric nitric acid as observed in the winter polar regions [*Frahm et al.*, 1997; *Sharber et al.*, 1998]. The purpose of the present work is to quantify, from first principles, the production of bremsstrahlung photons during energetic electron precipitation events, as well as the resultant ionization production and atmospheric chemistry effects. By modeling the subsequent propagation of bremsstrahlung photons in the atmosphere, this paper provides a means towards better interpretation of the X-ray measurements by the Balloon Array for RBSP Relativistic Electron Losses (BARREL) [*Millan et al.*, 2013].

2 Model Formulation

Three numerical models are employed in the present study: the Energetic Precipitation Monte Carlo model (EPMC) [*Lehtinen et al.*, 1999], the Monte Carlo model for Photons (MCP) [*Xu et al.*, 2012], and the Sodankylä Ion and Neutral Chemistry (SIC) model [*Turunen et al.*, 1996; *Verronen et al.*, 2005]. Specifically, the effects brought by bremsstrahlung photons during EEP are quantified in two steps. First, using the two Monte Carlo models, we simulate the interaction of precipitating electrons with the atmosphere and calculate the altitude profiles of ionization rates by both primary precipitating electrons and secondary bremsstrahlung photons. Second, the ionization rate profile is used as the input to the SIC model in order to estimate the resultant atmospheric changes. We mainly focus on the relative changes in the molecular concentration ("concentration" used in the following for simplicity) of odd hydrogen ($[HO_x] = [H] + [OH] + [HO_2]$), odd nitrogen ($[NO_x] = [N] + [NO] + [NO_2]$), and odd oxygen ($[O_x] = [O] + [O_3]$). The main collisional processes involved in EEP, together with the illustration of balloon-, ground-, and space-based measurements, are schematically depicted in Figure 1a.

In the first step of Monte Carlo simulations, monoenergetic beams of energetic electrons are assumed to precipitate into the upper atmosphere with discrete pitch angles (0° or 45°). The EPMC model is first used to calculate the energy deposition along the particle's path of propagation and the production of bremsstrahlung photons. The transport of bremsstrahlung photons, as well as the production of energetic electrons via photoelectric absorption and Compton scattering, is further simulated using the MCP model. Finally, we employ the EPMC model again in order to simulate the propagation of these bremsstrahlung-induced energetic electrons. The energy deposition by precipitating and bremsstrahlung-induced electrons is calculated as a function of altitude and the ionization rate is derived by assuming that it takes ~35 eV to produce an ion-electron pair [e.g., *Rees*, 1989, p. 40]. In the following, we describe the numerical models and the initial parameters used in the present simulations.

The EPMC model, adapted from the Monte Carlo model described in [*Lehtinen et al.*, 1999], is relativistic and three-dimensional (3D) in both configuration and velocity space. It models the propagation of electrons in the Earth's atmosphere by solving the equation of electron motion, i.e., the Langevin equation, within time steps [*Lehtinen et al.*, 1999]. The energy loss during electron propagation is described in terms of stopping power, i.e., dynamic friction force. The ionization collision is modeled using the Möller cross section and the magnetic mirroring force is explicitly included in this model. The angular scattering of electrons is mostly due to elastic scattering by air molecules, and the method of small-angle collisions is implemented as random changes to the momentum of electrons. The minimum energy threshold of this Monte Carlo model is set to be 2 keV. When its energy becomes lower than this threshold, the electron is removed from the simulation pool and assumed to deposit its energy locally. This minimum energy is valid given that we mainly focus on relativistic precipitating electrons in this study. By the time their energy becomes lower than 2 keV, these electrons have penetrated into significantly denser atmosphere and, therefore, would not propagate much further.

The geomagnetic field used in this model can be arbitrarily specified in direction and magnitude. In this study, it is assumed to be uniform and vertical with a magnitude of 41.5 μT. Due to the inclusion of a background magnetic field, the time step of electron simulation is primarily determined by the gyrofrequency at relatively high altitudes, and by the electron-neutral collision frequency at relatively low altitudes. For example, the breakeven altitude for the magnetization of 1 MeV electrons, at which the electron-neutral momentum loss rate is equal to the gyrofrequency, is approximately 30–35 km. For electrons with energy below 10 MeV, the radiative loss due to bremsstrahlung is negligible for the purpose of monitoring the electron energy [*Jackson*, 1975, p. 718]. The process of bremsstrahlung radiation is specifically modeled by factorizing the angular and energy parts of the outgoing photon [*Lehtinen*, 2000, pp. 45–49]. The differential cross sections are calculated using the Born approximation without considering the screening effect [*Heitler*, 1954, p. 245]. More details about this Monte Carlo model can be found in [*Lehtinen et al.*, 1999].

We simulate the transport of bremsstrahlung photons in the Earth's atmosphere, along with the production of energetic electrons via collisions of photons with air molecules, using the MCP model [*Xu et al.*, 2012]. This model takes into account three types of photon collisions that are dominant in the energy range between 10 keV and 100 MeV: photoelectric absorption, Compton scattering, and electron-positron pair production. We note that this model has been validated through various comparisons with results calculated using other numerical models in the studies of high-energy radiation from lightning discharges [e.g., *Xu et al.*, 2012, 2014, 2017]. Concerning the production of electrons, the electron binding energy is neglected in the process of photoelectric absorption and the outgoing photoelectron is assumed to have the same energy as the incident photon. The photoelectron momentum is determined using the relativistic form of the analytical angular differential cross section for photoelectric absorption processes [*Davisson and Evans*, 1952]. For Compton scattering, the energy and momentum of the electron knocked out are obtained using the conservation of momentum and energy.

After obtaining the altitude profiles of ionization rates using Monte Carlo simulations, the resultant changes in atmospheric neutral constituents are calculated using the SIC model. SIC is a 1-D atmospheric model that dynamically solves for the concentration of 16 minor neutral species and 72 ionic species in the altitude range between 20 and 150 km with 1 km resolution. Vertical motion of species is included as molecular and eddy diffusion, neglecting transport by prevailing neutral wind. The latest version of this model takes into account 389 ion-neutral and neutral-neutral reactions and 2523 ion-ion and electron-ion recombination reactions. The background profile of neutral density used in SIC modeling is obtained from the NRLMSISE-00 model [*Tobiska and Bouwer*, 2006] using the daily average values of solar radio flux ($F_{10.7}$) and the geomagnetic activity index (A_p). In addition to solar radiation, SIC is driven by external forces resulting from solar energetic particles, i.e., electron and proton precipitation, as well as galactic cosmic rays. In the present study, the background conditions in November 2012 at 65.14°N 147.44°W (Poker Flat, Alaska) are used in the SIC simulation. Chemical changes are calculated from 16 November 2012 22:00 UT until 19 November 00:00 UT and stored every 10 min of simulation. More details about this chemical model can be found in *Turunen et al.* [1996], *Verronen et al.* [2005], and *Verronen* [2006].

3 Results

3.1 Model Validation

The two Monte Carlo models used in the present study are first validated through the calculation of ionization rate and comparison with previously published results [*Frahm et al.*, 1997; *Fang et al.*, 2010], as shown in Figure 1. Figure 1b shows the comparison with the ionization rate profiles of monoenergetic electrons documented in *Fang et al.* [2010, Figure 2] for two energies: 100 keV and 1 MeV (labeled as "new method" in *Fang et al.* [2010, Figure 2]). The initial parameters of present simulations are chosen to be the same as those used in *Fang et al.* [2010]. In particular, the total incident energy of precip-

Figure 1. (a) Illustration of EEP interaction with the Earth's atmosphere, including processes of bremsstrahlung radiation, photoelectric absorption, and Compton scattering. Also shown in this figure is the illustration of balloon-, ground-, and space-based measurements. (b) Comparison of ionization rate profiles produced by beams of monoenergetic electrons between present modeling results and those reported in [*Fang et al.*, 2010, Figure 2]. The simulations are performed using the MSIS atmosphere with $F_{10.7}$ = 300 and A_p = 65. The total incident energy of precipitating electrons used in each simulation is 1 erg/cm^2/s. (c) Comparison of ionization rate profile between present modeling results and those presented in [*Frahm et al.*, 1997, Figure 1]. The dashed curve shows the bremsstrahlung-induced ionization rate. The energy distribution and fluxes of precipitating electrons used in this simulation are obtained from [*Frahm et al.*, 1997, Plate 1].

Figure 2. (a) The number of bremsstrahlung photons, as well as energetic electrons knocked out during processes of photoelectric absorption and Compton scattering, produced per precipitating electron injected per km by the monoenergetic beam of 1 MeV electrons with a pitch angle of 0°. (b) Energy distributions of bremsstrahlung photons produced by monoenergetic beams of precipitating electrons at different altitudes for three representative energies: 100 keV, 1 MeV, and 10 MeV. The distributions are normalized so that the integration over photon energy yields unity. (c) Energy distributions of photoelectrons and Compton electrons produced at the altitude of BARREL payload (35±1 km) by the monoenergetic beam of 1 MeV electrons with a pitch angle of 0°. (d) Altitude profiles of ionization rate produced by monoenergetic beams of precipitating electrons and their secondary bremsstrahlung photons, for three representative energies: 100 keV, 1 MeV, and 10 MeV, and two pitch angles: 0° and 45°. The total energy of source precipitating electrons used in each simulation is 1 erg/cm^2/s.

itating electrons used in each simulation is 1 erg/cm^2/s and the background density profile is calculated using the MSIS-90 model [*Tobiska and Bouwer*, 2006] with $F_{10.7}$ = 300 and A_p = 65. Monoenergetic beams of energetic electrons are propagated from an altitude of 300 km and the beaming of these electrons is assumed to be isotropic within the loss cone. In spite of the fundamental difference between Monte Carlo simulation and multi/two-stream modeling, present results show fairly good agreements with [*Fang et al.*, 2010]. The altitude of peak ionization rate, as well as the maximum value, are slightly lower than *Fang et al.* [2010]. We note that this discrepancy is likely due to the difference in the stopping power and the assumption of angular scattering used in EPMC.

We have also validated the simulation of bremsstrahlung radiation and resultant ionization production by comparing with the results presented in *Frahm et al.* [1997, Figure 1], as shown in Figure 1c. The dashed curve shows the bremsstrahlung-induced ionization rate and the solid curve shows the total ionization resulting from precipitating electrons. For the sake of direct comparison, the energy distribution and fluxes of source precipitating electrons are obtained from [*Frahm et al.*, 1997, Plate 1]. These electrons are also assumed to precipitate from an altitude of 300 km and the beaming is assumed to be isotropic. As clearly shown in this figure, both the direct impact ionization, at altitudes above ~50 km, and the bremsstrahlung-induced ionization, at altitudes below ~50 km, show good agreements with [*Frahm et al.*, 1997]. Moreover, the altitude of peak ionization rate and the minimum altitude where bremsstrahlung photons deposit their energy are consistent with [*Frahm et al.*, 1997]. Note also that the set of electron and photon cross sections used in the present calculation might be different from [*Frahm et al.*, 1997].

3.2 Ionization Effects

Figure 2a shows the altitude distribution of bremsstrahlung photons produced by the beam of 1 MeV electrons, when injected into the atmosphere from 300 km altitude with a pitch angle of 0°. Also shown in this figure is the altitude distribution of the energetic electrons knocked out during processes of photoelectric absorption and Compton scattering by bremsstrahlung photons. These distributions are normalized so that the integration over altitude is the total number produced per precipitating electron injected in the Monte Carlo simulation. Approximately 0.5% of the total precipitation energy is converted into bremsstrahlung production for 1 MeV incident electron energy. The number of photoelectrons and Compton electrons produced per precipitating electron is approximately 0.14 and 0.15, respectively. In addition, one sees that photoelectrons are mostly produced at altitudes close to the production altitude of bremsstrahlung photons, whereas Compton electrons are produced at considerably lower altitudes. In this example, the altitudes of peak production rate for photoelectrons and Compton electrons are ~56 km and ~30 km, respectively, while the altitude of peak bremsstrahlung production is ~58 km.

By collecting all the bremsstrahlung photons produced by precipitating electrons at different altitudes, we have also calculated the energy distributions of bremsstrahlung photons for three electron energies: 100 keV, 1 MeV, and 10 MeV, as shown in Figure 2b. The integration over photon energy yields unity. Figure 2c shows the energy distributions of those energetic electrons produced at the altitude of BARREL payload (35±1 km) by the bremsstrahlung photons originating from the monoenergetic beam of 1 MeV electrons with a pitch angle of 0°. The distribution is normalized so that the integration over electron energy yields unity and the partial energy distributions of photoelectrons and Compton electrons are also presented as dashed lines. The average energies of photoelectrons and Compton electrons are 36.8 keV and 40.8 keV, respectively. Before being absorbed by the atmosphere, the average number of photoelectrons and Compton electrons produced between 34 and 36 km altitude, representing the altitude of BARREL campaign, per precipitating electron is approximately 6.8×10^{-4} and 4.4×10^{-3}, respectively, for the 1 MeV case.

Figure 2d shows modeling results of altitude profiles of the ionization rates produced by monoenergetic beams of precipitating electrons and their secondary bremsstrahlung photons. The ionization profiles are calculated for three representative energies: 100 keV, 1 MeV, and 10 MeV, and two pitch angles: 0° and 45°. We see that, first, the altitude of peak ionization rate depends on the pitch angle by up to a few kilometers. Second, as better illustrated in the results of 100 keV electrons with a pitch angle of 0°, the ionization profile consists of three peaks: one due to the direct impact ionization at ~80 km altitude, one due to photoelectrons at ~58 km altitude, and another one due to Compton electrons at ~40 km altitude.

A direct comparison between Figure 2a and Figure 2d shows that the bremsstrahlung-induced ionization closely follows the altitude distribution of photoelectrons and Compton electrons. This is because these bremsstrahlung-induced electrons cannot propagate significantly downward into the denser atmosphere. For example, the attenuation length of 10 MeV electrons in the ambient air density at 20 km altitude is only ~590 m [e.g., *Suszcynsky et al.*, 1996]. Thanks to the bremsstrahlung photons, energetic precipitating electrons are capable of ionizing air molecules at altitudes significantly lower than the direct impact ionization. However, the ionization production by bremsstrahlung photons is much weaker than that of precipitating electrons. Even for 10 MeV precipitating electrons, the bremsstrahlung-induced ionization is two orders of magnitude weaker than the direct impact ionization.

3.3 Chemical Effects

Figure 3 shows SIC modeling results of, from top to bottom, electron concentration with the unit of cm^{-3} and relative changes in NO_x, HO_x, and O_x. The relative changes are the fraction of concentrations between simulation results with and without applying the external electron forcing and, thus, unitless. The results are obtained by applying an elec-

Figure 3. SIC modeling results of (a) electron concentration with the unit of cm^{-3} and relative changes of (b) NO_x, (c) HO_x, and (d) O_x, i.e., the fraction of concentrations between simulation results with and without applying the external electron forcing. The results are obtained by applying an electron forcing at 04:40 UT on 17 November with an intensity of 1 erg/cm^2/s lasting for 120 min, as denoted by dashed lines. The ionization rate profiles produced by the monoenergetic beam of 1 MeV electrons with a pitch angle of 0° are used as external electron forcing in this simulation. The left panels are calculated using the ionization profile without considering the bremsstrahlung process, while the right panels correspond to the ionization profile with the bremsstrahlung process taken into account. The simulations are performed using the background conditions in November 2012 at 65.14°N 147.44°W (Poker Flat, Alaska).

Figure 4. Same as Figure 3, but calculated using the ionization profiles of 10 MeV precipitating electrons.

tron forcing at 04:40 UT on 17 November with an intensity of 1 erg/cm^2/s lasting for 120 min, as denoted by dashed lines. The ionization rate profiles produced by the monoenergetic beam of 1 MeV electrons with a pitch angle of 0° are used as external electron forcing in this simulation. The left panels are calculated using the ionization profile without considering the bremsstrahlung process, while the right panels correspond to the ionization profile with the bremsstrahlung process taken into account. Figure 4 shows similar results, but calculated using the atmospheric ionization profiles of 10 MeV electrons with a pitch angle of 0°. This simulation represents an extremely intense event of relativistic electron precipitation and is conducted in order to evaluate the maximum possible atmospheric effects that can be induced by bremsstrahlung photons. Note that, different from the relative changes of NO_x and HO_x, the colorbar of O_x change is inverted in order to show the concentration decrease.

For both the 1 MeV and 10 MeV simulations, the electron density is first enhanced by orders of magnitude during the electron forcing. Due to the efficient electron-ion recombination process, this density promptly returns to the normal diurnal cycle after the electron forcing. Because of the ionization production, the concentration of NO_x significantly increases at altitudes of direct impact ionization. For example, as shown in Figure 4, the NO_x increases dramatically between ∼40 and ∼75 km for the ionization profile of 10 MeV electrons. The largest enhancement of NO_x concentration is approximately a factor of 8.3 and occurs around 72 km. After the electron forcing, the NO_x recovery is mainly due to the photodestruction of NO, which is gradual and relatively slow [*Turunen et al.*, 2016]. About 71% of the excess NO_x produced by the forcing of 10 MeV monoenergetic electrons at ∼72 km remains beyond the end of the 2-day simulation period (see Figure 4). However, as evident in Figure 3 and Figure 4, bremsstrahlung-induced ionization does not lead to notable changes in NO_x concentration at altitudes below 40 km, despite the visible electron density enhancement at these altitudes in Figures 3 and 4.

Unlike the changes in NO_x, HO_x is enhanced not only by direct impact ionization, but also by bremsstrahlung-induced ionization, as better shown in the 10 MeV simulation (Figure 4). At altitudes between ∼35 and ∼80 km, HO_x concentration is enhanced by up to a factor of 132 because of the direct ionization by precipitating electrons. Above 85 km, the density of water vapor rapidly decreases with increasing altitude, therefore limiting the production of ionic HO_x [*Turunen et al.*, 2016]. The largest enhancement of HO_x by bremsstrahlung-induced ionization is approximately a factor of 83 at ∼29 km. As for the external forcing of 1 MeV electrons, the largest increase due to bremsstrahlung-induced ionization is approximately a factor of 8.7. After the electron forcing, the recovery of HO_x due to chemical loss is much faster than NO_x and, therefore, does not have the long "tail" as in the results of NO_x change.

Concerning the relative changes in O_x, its concentration decreases at the altitudes of direct impact ionization. The decrease is mainly caused by the loss due to enhanced HO_x catalytic cycles [*Turunen et al.*, 2016]. These cycles require atomic oxygen to be effective, and atomic oxygen below 80 km is abundant only during sunlit hours when produced in O_2 photodissociation. For this reason, the O_x loss by electron-enhanced HO_x occurs during sunrise and especially during sunset hours when enough atomic oxygen is available for catalytic cycles [*Turunen et al.*, 2016]. A direct comparison between the SIC simulations with and without considering the bremsstrahlung effects shows that the bremsstrahlung-induced ionization has almost negligible impact on O_x concentration.

4 Discussion

Using Monte Carlo simulations of the EEP interaction with the Earth's atmosphere, we have studied the energy deposition and ionization production by both precipitating electrons and their secondary bremsstrahlung photons. The simulated ionization rate profiles are in excellent agreement with the results of [*Fang et al.*, 2010] for monoenergetic electrons, and with the results of [*Frahm et al.*, 1997] when the process of bremsstrahlung radiation is taken into account. Using the ionization rate profile as external forcing in the SIC model, we have further quantified the resultant changes in atmospheric neutral constituents.

Photoelectric absorption is the main collisional process for photons with energies below ~30 keV, while Compton scattering is dominant in the energy range between ~30 keV and ~30 MeV. Because of this difference, electrons knocked out through the process of Compton scattering, when compared with photoelectrons, are produced by more energetic photons. These more energetic photons can propagate further distances in the atmosphere before being eventually absorbed, corresponding to the production of Compton electrons at lower altitudes (see Figure 2a). Another consequence of this difference has been extensively observed by BARREL: a significant amount of low-energy photons would be absorbed by the atmosphere before penetrating into the stratosphere, thereby leading to the reduction of X-ray flux in the energy range below ~30 keV [e.g., *Woodger et al.*, 2015; *Clilverd et al.*, 2017]. Furthermore, as shown in Figure 2b, large quantities of photoelectrons and Compton electrons also can be produced at the altitude of the BARREL payloads. As the secondary effect of EEP, measurements of these bremsstrahlung-induced electrons, especially the altitude distribution, could be used as a means to explore precipitation properties.

The transport of precipitating electron energy in the form of bremsstrahlung photons leads to ionization at altitudes significantly lower than the direct impact ionization, as low as ~20 km for 1 MeV precipitating electrons (see Figure 2d). This is because the attenuation length of bremsstrahlung photons is much longer than energetic electrons. Moreover, as the energy of precipitating electrons increases from 100 keV to 10 MeV, the process of bremsstrahlung radiation becomes more efficient, leading to more energy deposition and ionization production in the atmosphere. This effect can be readily observed in Figure 2d. The difference between the direct impact and bremsstrahlung-induced ionization corresponding to the electron energy of 10 MeV is significantly smaller than the 100 keV case. The fraction of the total precipitation energy that is transferred into bremsstrahlung photons is mainly determined by the energy of precipitating electrons. Therefore, the X-ray fluxes measured in the stratosphere, as well as associated energetic electrons, provide valuable information about the energetics of the precipitation source.

As shown in Figure 4, even with the 120-min external forcing of 10 MeV monoenergetic electrons, the atmospheric chemistry effects of bremsstrahlung-induced ionization are likely insignificant. The ionization production by bremsstrahlung photons during EEP is significantly weaker than the direct impact ionization. The energy deposited by bremsstrahlung photons causes rapid and localized enhancements in electron and HO_x

concentration. The largest enhancement of HO_x concentration due to bremsstrahlung-induced ionization is approximately 83 and 8.7 times the background concentration for 10 MeV and 1 MeV monoenergetic electrons, respectively. Nevertheless, SIC modeling results suggest that the bremsstrahlung effect does not lead to substantial changes in NO_x and O_x concentrations.

Acknowledgments

This research was supported by the NSF grants AGS-1243176 and AGS-1732359. A.K. was supported by European Regional Development Fund (Regional Council of Lapland, decision number A70179). The simulation data and analysis codes used to generate all figures and results in this paper are available at https://github.com/wexu6668/EEP_GRL_2017.

References

Andersson, M. E., P. T. Verronen, C. J. Rodger, M. A. Clilverd, and A. Seppälä (2013), Missing driver in the Sun-Earth connection from energetic electron precipitation impacts mesospheric ozone, *Nat. Commun.*, *5*, 5197–5197, doi:10.1038/ncomms6197.

Barr, R., D. L. Jones, and C. Rodger (2000), ELF and VLF radio waves, *J. Atmos. Solar Terr. Phys.*, *62*, 1689–1718.

Clilverd, M. A., C. J. Rodger, M. McCarthy, R. Millan, L. W. Blum, N. Cobbett, J. B. Brundell, D. Danskin, and A. J. Halford (2017), Investigating energetic electron precipitation through combining ground-based, and balloon observations, *J. Geophys. Res. Space Physics*, *122*, doi:10.1002/2016JA022812.

Cotts, B. R. T., U. S. Inan, and N. G. Lehtinen (2011), Longitudinal dependence of lightning-induced electron precipitation, *J. Geophys. Res.*, *116*, A10206, doi:10.1029/2011JA016581.

Davisson, C. M., and R. D. Evans (1952), Gamma-Ray Absorption Coefficients, *Rev. Mod. Phys.*, *24*, 79–107.

Fang, X., C. E. Randall, D. Lummerzheim, S. C. Solomon, M. J. Mills, D. R. Marsh, C. H. Jackman, W. Wang, and G. Lu (2008), Electron impact ionization: A new parameterization for 100 eV to 1 MeV electrons, *J. Geophys. Res.*, *113*, A09311.

Fang, X., C. E. Randall, D. Lummerzheim, W. Wang, G. Lu, S. C. Solomon, and R. A. Frahm (2010), Parameterization of monoenergetic electron impact ionization, *Geophys. Res. Lett.*, *37*, L22106, doi:10.1029/2010GL045406.

Frahm, R. A., J. D. Winningham, J. R. Sharber, R. Link, G. Crowley, E. E. Gaines, D. L. Chenette, B. J. Anderson, and T. A. Potemra (1997), The diffuse aurora: A significant source of ionization in the middle atmosphere, *J. Geophys. Res.*, *102*(D23), 28,203–28,214, doi:10.1029/97JD02430.

Garcia, R. R., D. R. Marsh, D. E. Kinnison, B. A. Boville, and F. Sassi (2007), Simulation of secular trends in the middle atmosphere, 1950–2003, *J. Geophys. Res.*, *112*, D09301, doi:10.1029/2006JD007485.

Heitler, W. (1954), *The Quantum Theory of Radiation*, 3rd ed., Clarendon, Oxford.

Jackson, J. D. (1975), *Classical Electrodynamics*, 2 ed., John Wiley, New York.

Lazarev, V. I. (1967), Absorption of the energy of an electron beam in the upper atmosphere, *Geomagn. Aeron.*, *7*, 219.

Lehtinen, N. G. (2000), Relativistic runaway electrons above thunderstorms, Ph.D. thesis, Stanford Univ., Stanford, CA.

Lehtinen, N. G., T. F. Bell, and U. S. Inan (1999), Monte Carlo simulation of runaway MeV electron breakdown with application to red sprites and terrestrial gamma ray flashes, *J. Geophys. Res.*, *104*(A11), 24,699–24,712, doi:10.1029/1999JA900335.

Lummerzheim, D. (1992), Comparison of energy dissipation functions for high energy auroral electron and ion precipitation, *Rep. UAG-R-318*, pp. Geophys. Inst., Univ. of Alaska Fairbanks, Fairbanks.

Millan, R. M., et al. (2013), The balloon array for RBSP relativistic electron losses (BARREL), *Space Sci. Rev.*, *179*, 503–530, doi:10.1007/s11214-013-9971-z.

Randall, C. E., et al. (2007), Energetic particle precipitation effects on the Southern Hemisphere stratosphere in 1992–2005, *J. Geophys. Res.*, *112*, D08308, doi:10.1029/2006JD007696.

Rees, M. H. (1989), *Physics and Chemistry of the Upper Atmosphere*, Cambridge Univ. Press, New York.

Roble, R. G., and E. C. Ridley (1987), An auroral model for the NCAR thermospheric general circulation model (TGCM), *Ann. Geophys.*, *5A*, 369–382.

Rozanov, E., M. Calisto, T. Egorova, T. Peter, and W. Schmutz (2012), Influence of the precipitating energetic particles on atmospheric chemistry and climate, *Surv. Geophys.*, *33*, 483–501, doi:10.1007/s10712-012-9192-0.

Rusch, D. W., J.-C. Gerard, S. Solomon, P. J. Crutzen, and G. C. Reid (1981), The effect of particle precipitation events on the neutral and ion chemistry of the middle atmosphere–I. Odd nitrogen, *Planet. Space Sci.*, *29*(7), 767–774, doi:10.1016/0032-0633(81)90048-9.

Seppälä, A., M. A. Clilverd, M. J. Beharrell, C. J. Rodger, P. T. Verronen, M. E. Andersson, and D. A. Newnham (2015), Substorm-induced energetic electron precipitation: Impact on atmospheric chemistry, *Geophys. Res. Lett.*, *42*, 8172–8176, doi:10.1002/2015GL065523.

Sharber, J. R., et al. (1998), UARS particle environment monitor observations during the November 1993 storm: Auroral morphology, spectral characterization, and energy deposition, *J. Geophys. Res.*, *103*(A11), 26,307–26,322, doi:10.1029/98JA01287.

Sinnhuber, M., H. Nieder, and N. Wieters (2012), Energetic particle precipitation and the chemistry of the mesosphere/lower thermosphere, *Surv. Geophys.*, *33*, 1281–1334, doi:10.1007/s10712-012-9201-3.

Solomon, S., D. W. Rusch, J.-C. Gérard, G. C. Reid, and P. J. Crutzen (1981), The effect of particle precipitation events on the neutral and ion chemistry of the middle atmosphere: II. Odd hydrogen, *Planet. Space Sci.*, *29*(8), 885–893, doi:10.1016/0032-0633(81)90078-7.

Solomon, S. C. (2001), Auroral particle transport using monte carlo and hybrid methods, *J. Geophys. Res.*, *106*(A1), 107–116, doi:10.1029/2000JA002011.

Suszcynsky, D. M., R. Roussel-Dupre, and G. Shaw (1996), Ground-based search for X rays generated by thunderstorms and lightning, *J. Geophys. Res.*, *101*(D18), 23,505–23,516, doi:10.1029/96JD02134.

Thorne, R. M. (1980), The importance of energetic particle precipitation on the chemical composition of the middle atmosphere, *PAGEOPH*, *118*, 128–151, doi:0.1007/BF01586448.

Tobiska, W. K., and S. D. Bouwer (2006), New developments in solar2000 for space research and operations, *Adv. Space Res.*, *37*, 347–358, doi:10.1016/j.asr.2005.08.015.

Turunen, E., H. Matveinen, J. Tolvanen, and H. Ranta (1996), D-region ion chemistry model, in *STEP Handbook of Ionospheric Models*, edited by R. W. Schunk, pp. 1–25, SCOSTEP Secretariat, Boulder, Colorado.

Turunen, E., A. Kero, P. T. Verronen, Y. Miyoshi, S.-I. Oyama, and S. Saito (2016), Mesospheric ozone destruction by high-energy electron precipitation associated with pulsating aurora, *J. Geophys. Res. Atmos.*, *121*, 11,852–11,861, doi:10.1002/2016JD025015.

Verronen, P. T. (2006), Ionosphere-atmosphere interaction during solar proton events, Ph.D. thesis, Univ. of Helsinki, Helsinki, Finland.

Verronen, P. T., A. Seppälä, M. A. Clilverd, C. J. Rodger, E. Kyrölä, C.-F. Enell, T. Ulich, and E. Turunen (2005), Diurnal variation of ozone depletion during the October–November 2003 solar proton events, *J. Geophys. Res.*, *110*, A09S32, doi:10.1029/2004JA010932.

Woodger, L. A., A. J. Halford, R. M. Millan, M. P. McCarthy, D. M. Smith, G. S. Bowers, J. G. Sample, B. R. Anderson, and X. Liang (2015), A summary of the BARREL campaigns: Technique for studying electron precipitation, *J. Geophys. Res. Space Physics*, *120*, 4922–4935, doi:10.1002/2014JA020874.

Xu, W., S. Celestin, and V. P. Pasko (2012), Source altitudes of terrestrial gamma-ray flashes produced by lightning leaders, *Geophys. Res. Lett.*, *39*, L08801, doi: 10.1029/2012GL051351.

Xu, W., S. Celestin, and V. P. Pasko (2014), Modeling of X-ray emissions produced by stepping lightning leaders, *Geophys. Res. Lett.*, *41*, 7406–7412, doi: 10.1002/2014GL061163.

Xu, W., S. Celestin, V. P. Pasko, and R. A. Marshall (2017), A novel type of transient luminous event produced by terrestrial gamma-ray flashes, *Geophys. Res. Lett.*, *44*, 2571–2578, doi:10.1002/2016GL072400.

Figure 1.

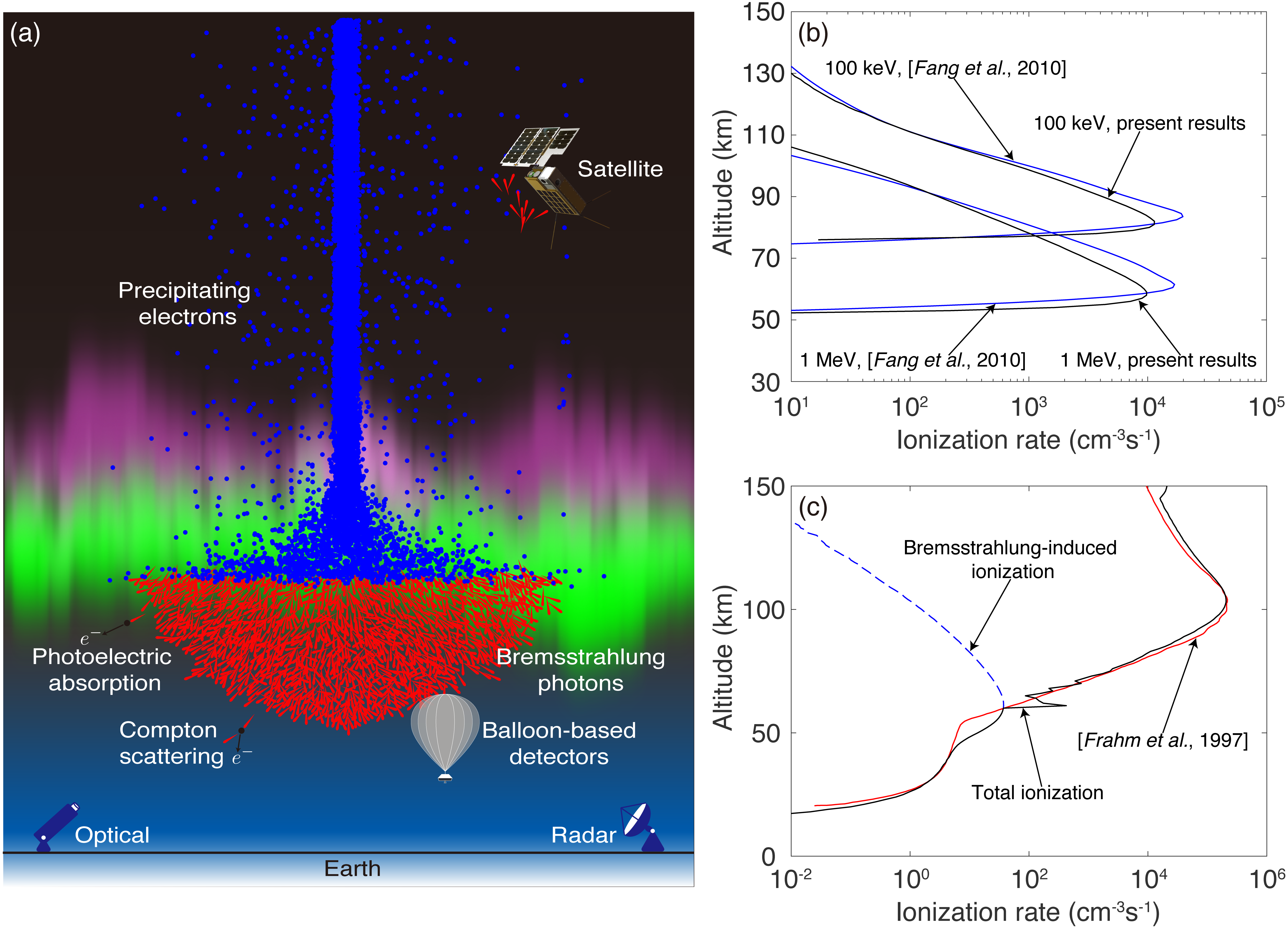
(a)
Satellite
Precipitating electrons
Photoelectric absorption
Bremsstrahlung photons
Compton scattering
Balloon-based detectors
Optical
Radar
Earth
(b)
100 keV, [Fang et al., 2010]
100 keV, present results
1 MeV, [Fang et al., 2010]
1 MeV, present results
Altitude (km)
Ionization rate (cm-3s-1)
(c)
Bremsstrahlung-induced ionization
[Frahm et al., 1997]
Total ionization
Altitude (km)
Ionization rate (cm-3s-1)

Figure 2.

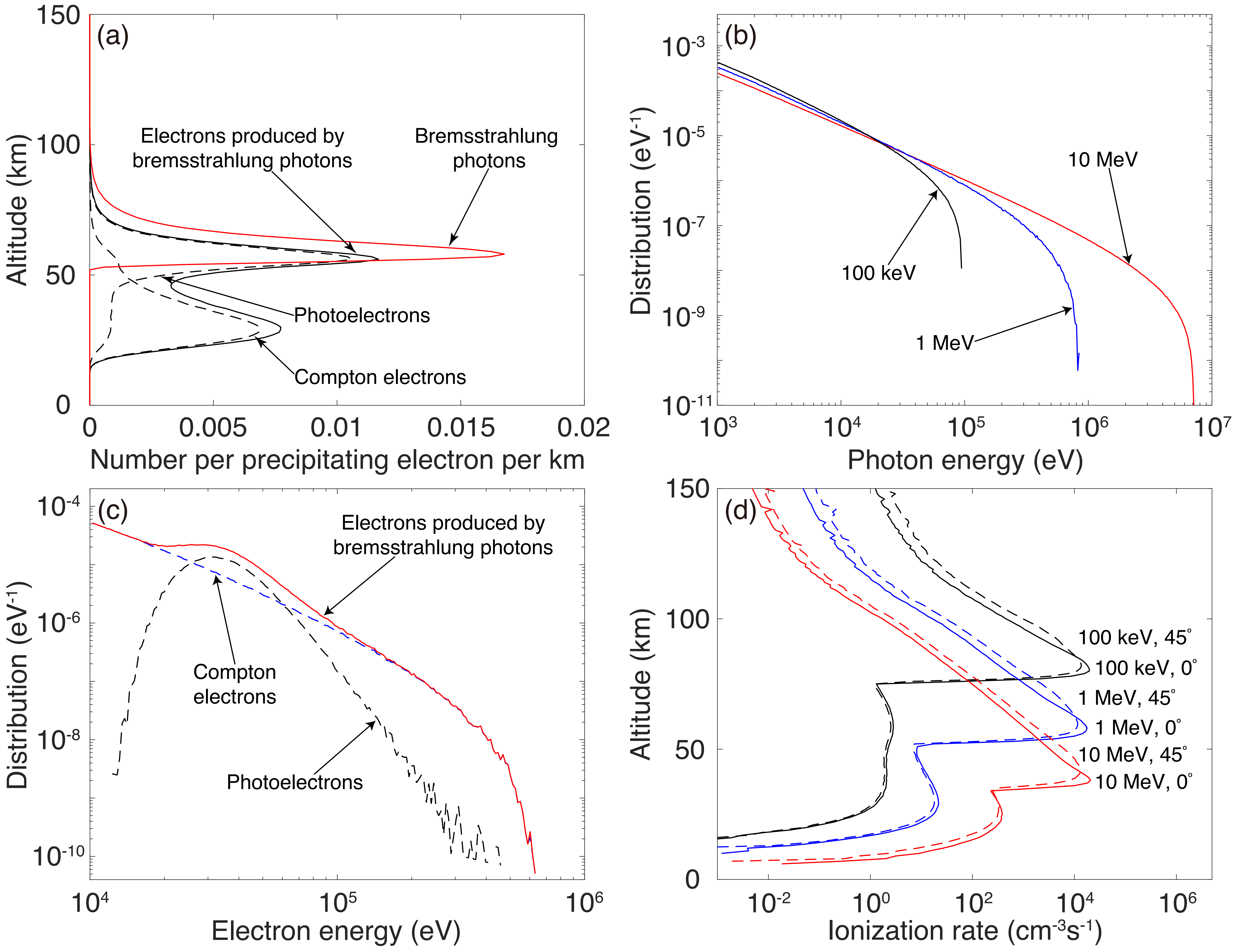

(a)
Electrons produced by bremsstrahlung photons
Bremsstrahlung photons
Photoelectrons
Compton electrons
Altitude (km)
Number per precipitating electron per km
(b)
10 MeV
100 keV
1 MeV
Distribution (eV^{-1})
Photon energy (eV)
(c)
Electrons produced by bremsstrahlung photons
Compton electrons
Photoelectrons
Distribution (eV^{-1})
Electron energy (eV)
(d)
100 keV, 45°
100 keV, 0°
1 MeV, 45°
1 MeV, 0°
10 MeV, 45°
10 MeV, 0°
Altitude (km)
Ionization rate (cm^{-3}s^{-1})

Figure 3.

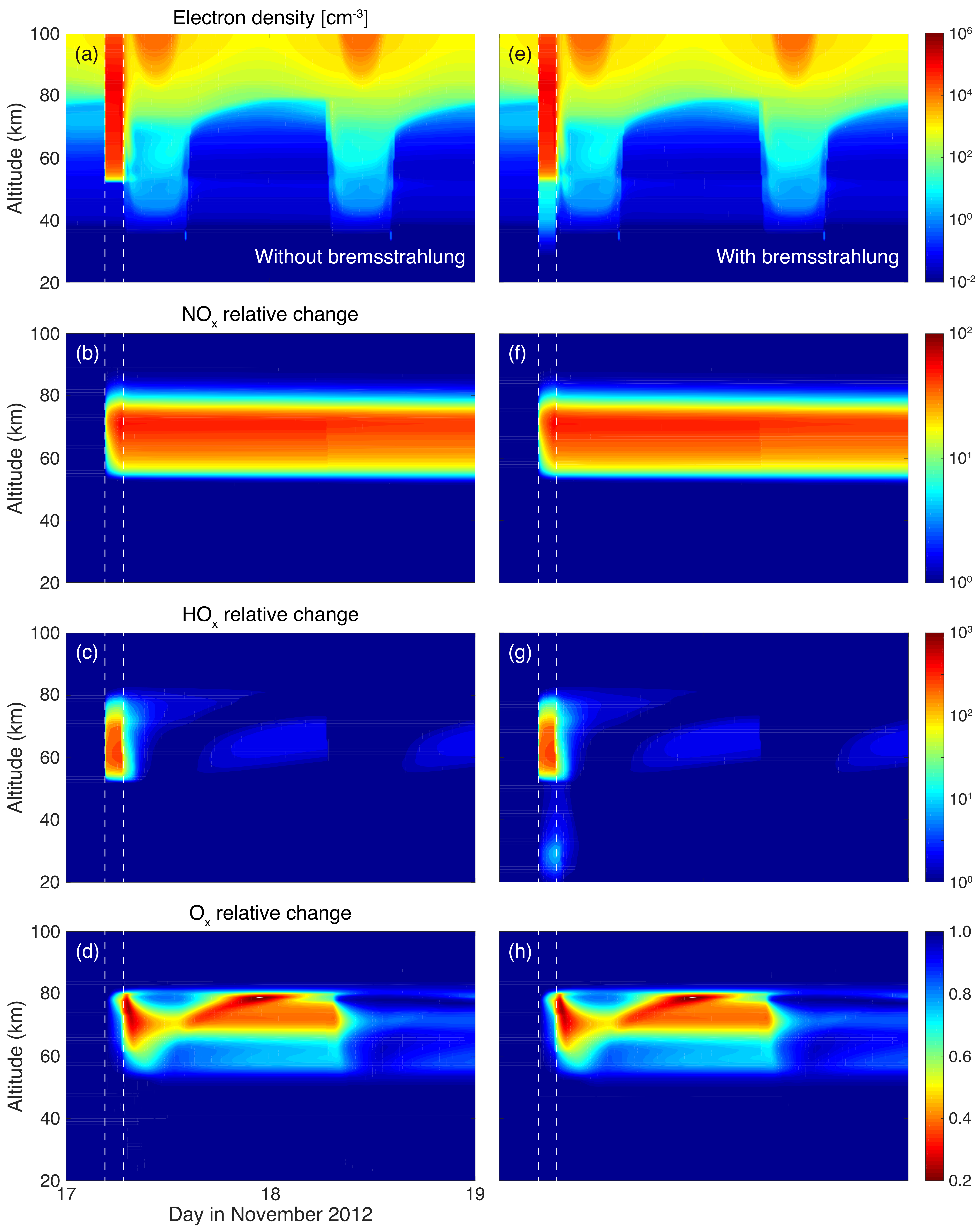

Electron density [cm^-3]
NO_x relative change
HO_x relative change
O_x relative change
(a)
(b)
(c)
(d)
(e)
(f)
(g)
(h)
Without bremsstrahlung
With bremsstrahlung
Altitude (km)
100
80
60
40
20
17
18
19
Day in November 2012
10^6
10^4
10^2
10^0
10^-2
10^2
10^1
10^0
10^3
10^2
10^1
10^0
1.0
0.8
0.6
0.4
0.2

Figure 4.

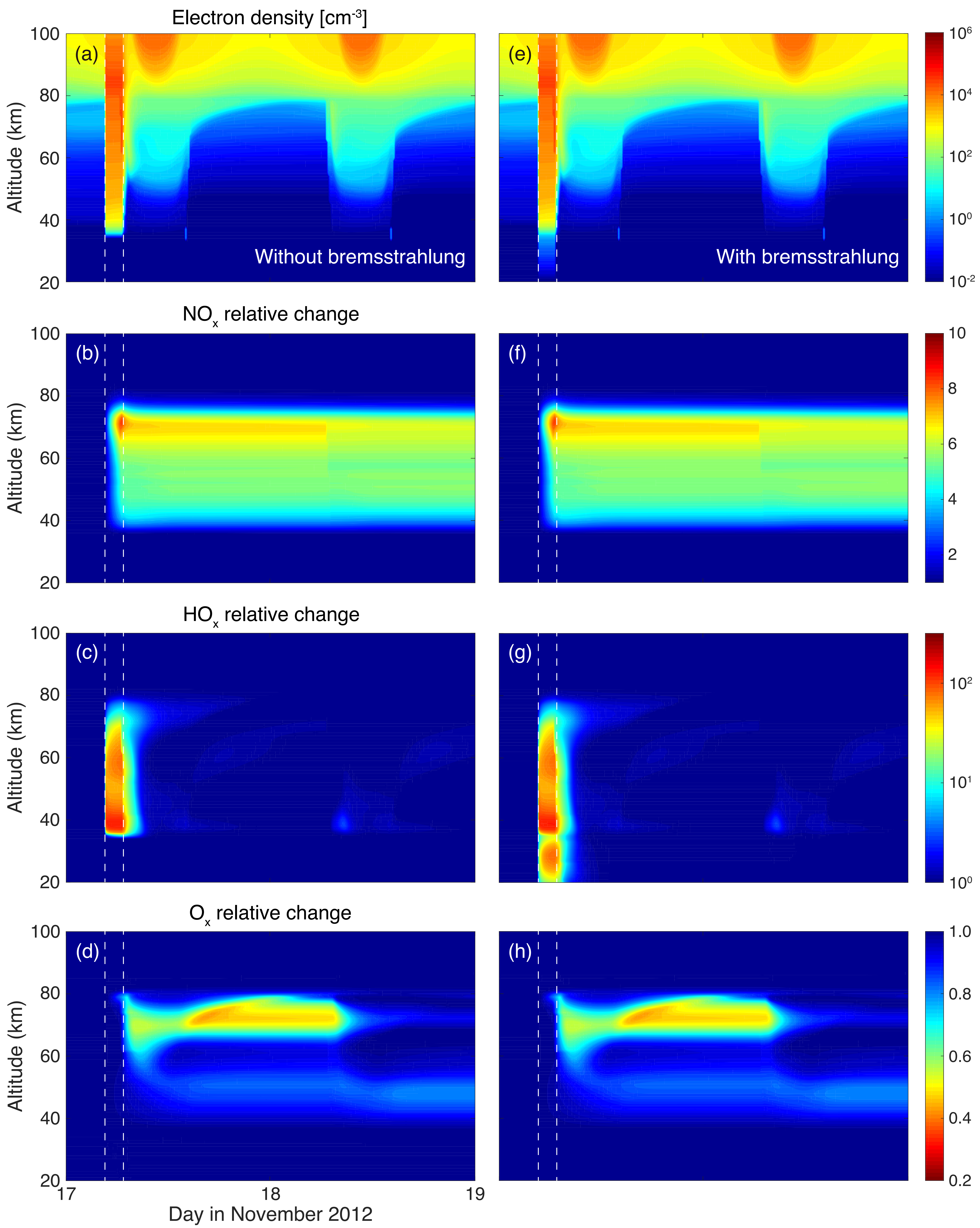

Electron density [cm^{-3}]
NO$_x$ relative change
HO$_x$ relative change
O$_x$ relative change
(a)
(b)
(c)
(d)
(e)
(f)
(g)
(h)
Without bremsstrahlung
With bremsstrahlung
Altitude (km)
Day in November 2012
17
18
19
20
40
60
80
100
10^6
10^4
10^2
10^0
10^{-2}
10
8
6
4
2
10^2
10^1
10^0
1.0
0.8
0.6
0.4
0.2